Impact hammer-based analysis of nonlinear effects in bolted lap joint

B. Titurus[1], J. Yuan[1,3], F. Scarpa[1], S. Patsias[2], S. Pattison[2]
[1] Department of Aerospace Engineering, University of Bristol, Queen's Building, University Walk, Bristol BS8 1TR, United Kingdom
e-mail: **brano.titurus@bristol.ac.uk**

[2] Rolls-Royce plc, PO Box 31, DE24 8BJ Derby, United Kingdom

[3] Department of Power and Propulsion, School of Aerospace, Transport and Manufacturing, Cranfield University, Bedfordshire, MK43 0AL, United Kingdom

Abstract
This work presents an experimental investigation into the dynamic behavior of a bolted joint beam configuration. The impact hammer is chosen as an alternative to classical harmonic excitation methods. The structural responses are explored for a range of the joint tightening toques and various levels of impulse hammer excitations. A symmetric beam assembly made of two nominally identical steel beams is studied. Symmetric modes are found to be sensitive to the test parameters. For given torque, impact-based varying joint loading conditions are used to induce the nonlinear joint effects. A linear data processing strategy is used to observe the nonlinear behavior indirectly. The dynamic joint behavior is described in the form of the modal frequency-damping ratio performance maps represented by the two-parametric approximating quadratic response surface models. This model maps the joint conditions on the corresponding dynamic characteristics of interest and it will serve as a basis for the parametric linear joint model development.

1 Introduction

The focus of this paper is on vibration-based analysis of bolted joints in beam assemblies. Such study is performed to support the development and validation of high performance Finite Element (FE) reduced order joint models. Bolted joints are commonly used to connect the separate structures in aerospace engineering, for example for the case of gas turbine engine. They are also one of the dominant fastening mechanisms for aerostructures subjected to intensive dynamic loads. It is therefore critical to understand the effect of the bolted joint parameters on the dynamic behavior of these connected structures. Significant damping in structures with bolted joints originates from the geometry, location and the position of the bolts. Every assembled interface involves various sources of uncertainty and nonlinearity resulting from friction and contact effects.

Vibration of aero-engine parts may result in failure through high cycle fatigue, in addition to the production of noise and discomfort for the passengers and crew. Aero-engine components are commonly subjected to high levels of vibration amplitudes excited under service conditions by aerodynamic and inertial forces. The excitations can have a very dense frequency spectrum and, similarly, the modal densities of the bladed disc can be also quite high. With careful design, it may be possible to minimize unwanted vibrations for a single operational frequency. However, these combined high spectrum excitation and modal densities make the task of avoiding all the resonance regimes almost impossible. Accurate prediction in forced response levels depends on the modeling of isolated components, and also on the modeling of the interaction forces between the components.

The friction caused by small relative motions between two components provides an important contribution to the damping in aero-engine structures such as blade disc systems [1,2]. These contact friction forces show a strongly nonlinear characteristics because of the slip-stick transitions, the influence of the normal force on the slip-stick transitions and the magnitude of the friction force and variation of contact area where slip occurs [1]. Furthermore, the variation of the contact area induced by the different vibration modes also leads to the variation of the stiffness properties of blade-disc joints over each vibration cycle, which can affect resonance frequencies of jointed structures. Understanding and including these nonlinear effects into the forced response analysis of bladed disk assemblies is therefore necessary.

Detailed finite element (FE) models are commonly used to describe realistic design features and to achieve practically acceptable accuracy in the forced response of bladed discs. However, the number of degrees of freedom in realistic FE models usually reaches millions and it makes the numerical cost of forced response calculations large, even in linear forced response calculations [1,3]. The nonlinear forced response analysis requires solution of bladed disks with friction contacts at the blade roots, which is however much numerically more expensive than the methods used for linear vibrations. Therefore, reduction techniques are demanding to make the use of feasible results in the linear system in the analysis of nonlinear vibrations system. In this way, the computational expense can be significantly reduced while it would not much compromise the accuracy of the prediction.

Bolted joint structures are quite crucial in aerospace engineering as they represent the dominant fastening mechanisms used in almost all primary parts, especially in the case of aero-engines. For the joint structure made of metal, its damping mainly derives from the dissipated energy through the contact friction in the bolted joint [2,4]. The contact friction in the bolted joint usually features as micro-slip friction because of the tightening torque between the two beams. Therefore, every assembled interface involves various sources of uncertainty and nonlinearity resulting from friction and contact effects. For this reason the local effects of damping should be considered along with the global effects arising from the material of the assembly. The complex behavior of these connecting elements play an important role in the overall dynamic characteristics of the structure, such as the modal damping ratio, natural frequencies, mode shapes and nonlinear response to external excitation. The effect of contact friction on the overall joined beam structure may be considered as being similar to the one present in a bladed disc system, especially when dovetails are used. Micro-slip friction exists in both bolted joints and bladed disc assemblies. The observation of the experimental data from the bolted joint structure will therefore provide a significant engineering insight of the micro-slip fiction from the physical point of view.

In this work the effect of the joint contact friction and its influence on the damping and natural frequencies of the beam structure is examined. The impact hammer is chosen as an alternative to classical harmonic excitation methods because of the minimum interaction with the tested structure. Impact is used to excite the structure and the resulting non-averaged free responses are used to study the joint in the frequency domain. In order to cover wide range of working conditions, the structural responses are explored for a range of joint tightening toques and impulse hammer excitations. The test case evaluated here is a simple symmetric beam. Symmetric and antisymmetric bending mode shapes are observed. The higher symmetric modes are increasingly sensitive to the joint conditions. This increasing modal sensitivity and the associated trends are studied and used to develop an insight into the physical processes inside the joint. These trends are then used to map the changing test parameters on the changes in the linear stiffness and damping joint descriptors. The mapping process is the primary source of modelling arguments explored in the later parts of the paper.

This paper is organized as follows: The experimental rig is introduced first, followed by the detailed description of test procedure and the data processing performed. The identified experimental data are then presented, commented and the quadratic response model is used to develop the approximating analytical model of the joint's modal frequency-damping performance map. Finally, a discussion and conclusion on the use of the response surface representation for the FE joint modelling is presented.

2 Methods and tools

2.1 Test structure

The experimental structure shown in Figure 1 consists of two nominally identical beams and one spring steel friction pad with two polished contact surfaces. The beams are made of steel with a nominal density of 7850 kg/m^3 and Young's modulus of 2.1×10^{11} Nm^{-2}. To enhance the observability of the contact and friction effects, the contact surfaces of the steel beams are roughened using sandblasting. All three parts are assembled using a single bolt and nut. As a result, the beam assembly has a joint located in the middle of its span. Both constituent beams have constant width of 25 mm.

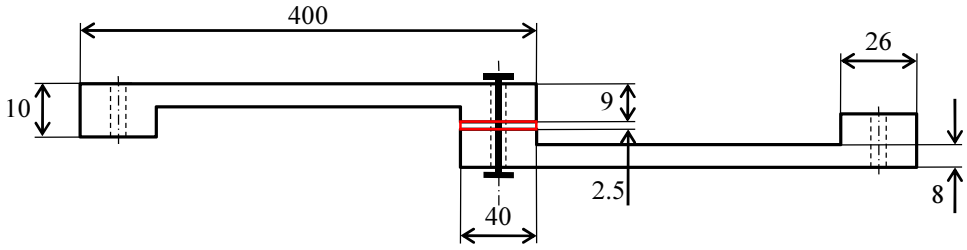

Figure 1: Experimental structure.

2.2 Test and signal processing procedure

The vibration tests were carried out in Bristol Laboratory of Advanced Dynamics Engineering at the University of Bristol. The horizontally placed structure was tested using free-free boundary conditions with the induced transversal vibration perpendicular to the plane of the suspension. An impact hammer (Bruel&Kjaer, model 086C01) was used to excite the structure at the tip of the beam assembly with the vibration response measured in the same place and direction using a piezoelectric accelerometer (PCB, model 333M07). The dynamic signal analyzer (National Instruments, model NI 9234) was used to acquire the data which were further processed in Matlab and its toolboxes (Matlab 2013a, Data Acquisition Toolbox Version 3.3) [5]. The frequency range of interest was chosen to be between 0 and 1000 Hz such that first five bending modes with three symmetric and two antisymmetric mode shapes were observed. The sampling frequency was 2048 Hz, the acquisition time 20 seconds and the hammer-determined effective excited frequency range was around 850 Hz. No windowing was used during the entire experiment process.

Single Input Single Output (SISO) process was used during the data post-processing stage. The time response acquired from the sensor was firstly converted into the response in the frequency domain using Discrete Fourier Transform (DFT) applied to the full response signals. Then, the output-input ratios were then constructed to represent the raw non-averaged acceleration frequency response functions (FRF). The details on how these transfer functions were further processed are described in the following section.

The *tightening torque* at the beam joint was used as the controlled test parameter. A hand-held dial torque wrench (Bahco, model 7454-3) with the range up to 3.5 Nm was used during the experiments. The value of the initial torques started from almost 0 Nm (small increment to ensure structural integrity during the tests), and then increased to 1.0, 2.1, 3.1 Nm by using the torque wrench with its manual control dial. The second test parameter is a peak *impact* force applied using the impact hammer. The hand-held impact hammer was used to observe the applied load patterns. During the tests weak and strong impacts were applied to excite the configuration at a range of peak force inputs. This crude method of input control is used to ensure that typically uncontrolled impact hammer excitation provides a full coverage of a wide input force range. Figure 2 shows the test configuration with the detail highlighting the joint area and the torque wrench.

Figure 2: Test structure with torque wrench and joint detail.

2.3 Modal analysis technique

Two test parameters are used here to induce the variable joint conditions. Changes in the tightening torque produce a non-stationary structural system. For given torque, impact-based varying joint loading conditions are used to induce the nonlinear joint effects. In this study, for given torque and peak impact hammer load, and because of the use of the stated signal processing strategy, the actual nonlinear behavior is not observed directly. Application of DFT to the full free vibration responses smears the time domain changes in the frequency content of the signals and produces, instead, a classical frequency spectra. The practical consequence of this process is that the fine time-dependent structure that is present in the raw time series is made unavailable, and only the most robust time-averaged performance characteristics of the joints are extracted. This research tries to determine the dynamic joint performance under these sub-optimal conditions. The resulting map between the conditions and dynamic characteristics should serve as the basis for the parametric linear joint model.

Identification automation was used to streamline the process due to large number of identification instances. This decision influenced the choice of simple and robust identification methods. As a part of the process, all identified linear vibration modes are assumed to be well separated and with low damping. This analysis, therefore, was focused on the identification of the equivalent modal parameters represented by the undamped natural frequencies and modal damping ratios for the first few flexible modes.

Firstly, automated circle fitting and natural frequency localization for given mode was performed in the specified frequency interval centered about the frequency associated with the maximum magnitude of the measured receptance FRFs. These data were used for the circle fitting based on the use of Kasa's method [6,7] which was applied to the measured mobility FRFs. The natural frequency was simply determined based on the maximum rate of change of the mobility phase angle specified relative to the circle's center.

The damping ratios were estimated based on the modified half-power bandwidth method. Owing to the assumption of small damping and good frequency separation each individual modal peak was processed about the identified natural frequency. The two values ω_1 and ω_2 were found based on the receptance FRF condition $|H(\omega)|=\alpha|H(\omega_j)|$, where ω_j is the natural frequency and $\alpha\in[0.3,0.6]$. The frequencies ω_1 and ω_2 were used to determine the damping ratio from the nonlinear equation $\omega_1^2-\omega_2^2=f(\alpha,\zeta_j)$. This equation established a map $\alpha\rightarrow\zeta_{j,\alpha}$ for given mode j and $|H(\omega)|$. This estimation process was repeated for a number of α-cutting levels. The final ζ_j was found as the arithmetic average of all intermediate $\zeta_{j,\alpha}$. Example of the results of this two-stage process is shown in Figure 3.

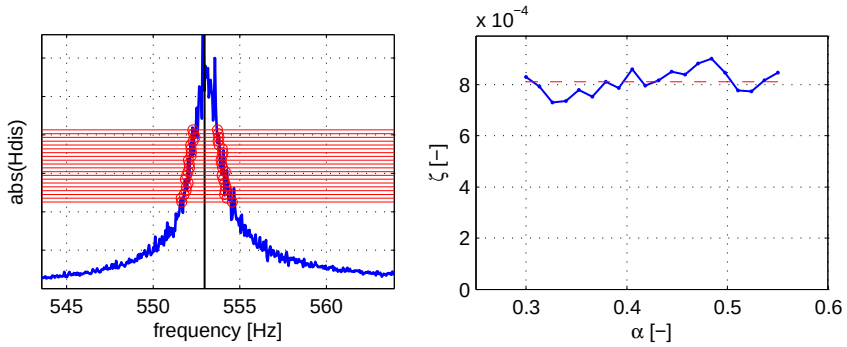

Figure 3: Example results of the two-stage natural frequency and damping ratio identification.

The identified ω_j and ζ_j for the selected FRFs were used to check the identification quality. The unknown residual terms were identified using the linear least square technique. A classical complex pole-parameterization [8] was used to find the residuals and to reconstruct the measured FRF

$$H(\omega_k) = \sum_{j=1}^{5} \left(\frac{R_j}{i\omega_k - \omega_j\zeta_j - i\,\omega_j\sqrt{1-\zeta_j^2}} + \frac{\overline{R}_j}{i\omega_k - \omega_j\zeta_j + i\,\omega_j\sqrt{1-\zeta_j^2}} \right) + \frac{T_R}{\omega_k^2} + E_R \tag{1}$$

where ω_k are the measured frequency points, ω_j and ζ_j is the j-th undamped natural frequency and modal damping ratio, R_j are the complex modal residuals, T_R, E_R are the complex out-of-the-range residual terms. Example of this reconstruction process in shown in Figure 4.

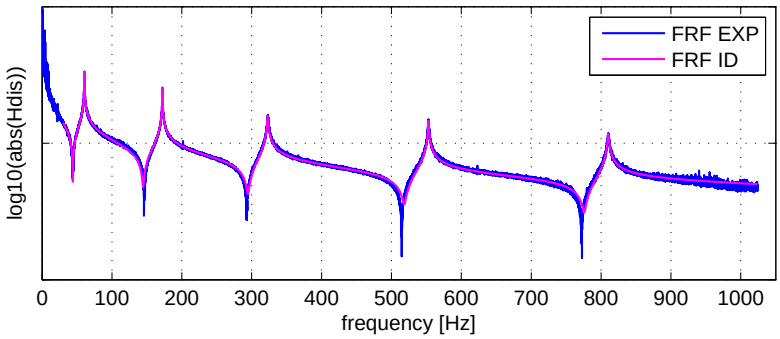

Figure 4: Example of FRF reconstruction.

2.4 Reference FE model

In order to understand the underlying modal shapes a reference FE model is created. Matlab code was used with 20 beam elements which combined uncoupled Euler-Bernoulli linear beam theory for the transversal and bending effects and the linear bar theory for the longitudinal effects. The point mass elements were used to model the effects of concentrated masses such as sensor or bolt-nut fastener. A pair of very stiff transversal and diagonal spring elements was used to model the joint at the highest levels of tightening torque. This model is shown in Figure 5.

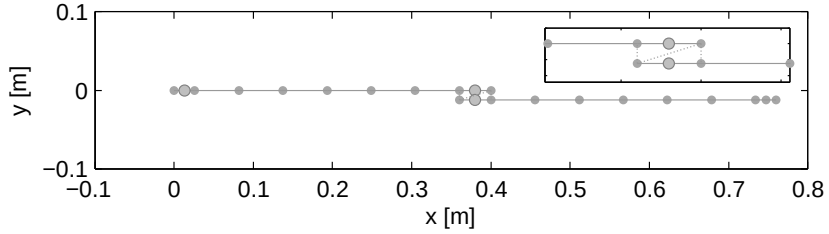

Figure 5: Reference FE model.

The frequency response of this model was calibrated against the measured data using the test case with the highest tightening torque and the lowest force inputs. The FRF-based calibration process involved changing the transversal spring element stiffness to k_y=1.15×10^8 N/m. The diagonal joint spring element influenced only the mode which represented the relative longitudinal motion of two beam substructures. The predicted natural frequencies were matched to the selected identified frequencies with the relative differences of - 2.21, -2.03, -1.16, -0.06 and -0.03% for the first five elastic modes. Summary comparison between the reference FE model and a set of all measured FRFs is shown in Figure 6.

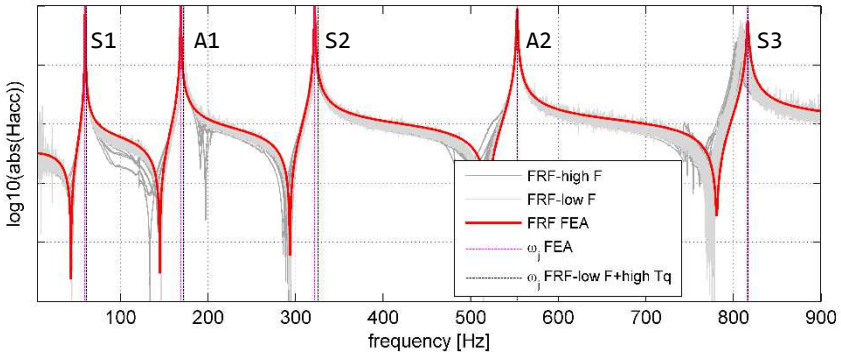

Figure 6: Calibrated reference FE model compared with the measured FRFs.

Elastic modes are shown in Figure 7. Symmetric and anti-symmetric bending modes are included. As reflected by the matched frequency results, the key reference mode is the fifth elastic denoted S3 in Figure 6. Due to its high modal curvature in the joint region this is the most sensitive mode and its dynamic parameters will be used as the main measure of joint conditions and behavior.

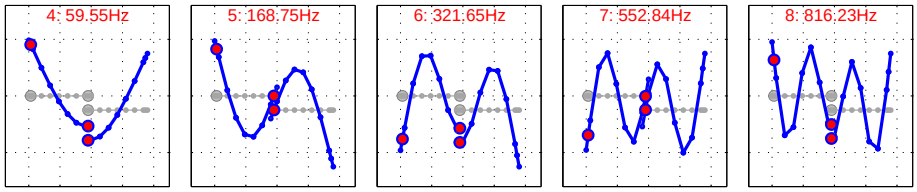

Figure 7: First five mode shapes of the calibrated reference FE model.

3 Results

3.1 Summary of the experimental cases

Five elastic modes were observed, four joint torque levels were tested and at least eight impact events were recorded for each torque level. Summary of these tests is shown in Figure 1. To enhance this graph, all modal peaks are shown in the same relative frequency interval of ±3% about the reference frequency which corresponds to the test with the highest tightening torque and the lowest impact force. It is clear that the symmetric modes S1, S2 and S3 feature high and comparable relative sensitivity to both test parameters.

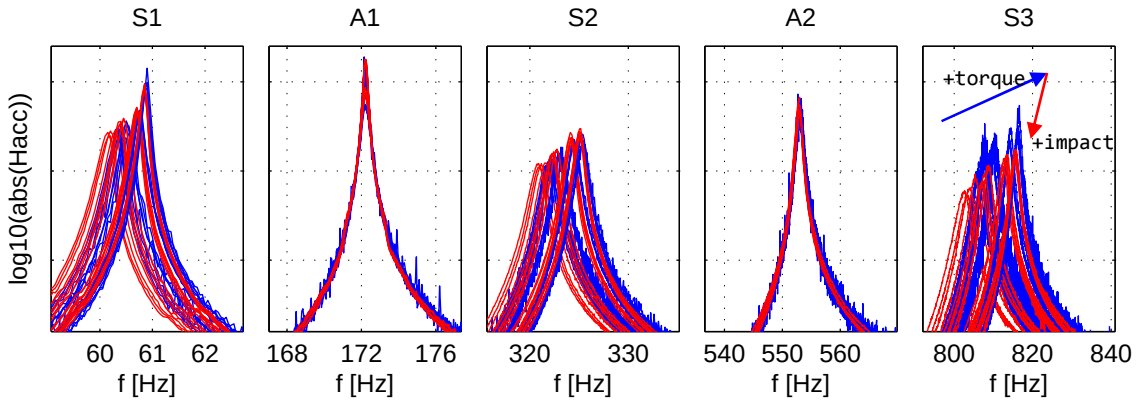

Figure 8: Influence of changing test conditions on the modal peaks (blue lines represent the low impact force tests and red lines represent the high impact force tests).

In total, at least 32 FRFs with 160 identifications are processed in order to gain insight into the dependencies between the modal properties and changing conditions. Figure 8 gives an indication about the observed trends caused by the varying joint conditions. For the sensitive modes, the increase in torque causes frequency increase (stiffening) with sharper modal peaks (lower modal damping). On the other hand, increase in the applied impact force produces FRFs with lower magnitudes of the modal peaks (higher modal damping) and negative frequency shift relative to the cases with low impact inputs (softening). While the cases with low force inputs represent better approximation of the linear “small vibration” conditions, they suffer from the increased presence of experimental noise and increased uncertainty. Further analysis of these results is based on the process presented in section 2.3.

3.2 Analysis of the identified modal properties

This section is used to summarize all identified results. Figure 9 shows the relationships between the maximum impact forces and the natural frequencies for all elastic modes. Each case of the tightening torque is identified by the color and different markers are used to differentiate the cases with strong and weak hammer inputs. The text labels also identify individual torque cases. Error ellipse is used to highlight the different torque clusters and their trends with increasing impact loads. To facilitate visual comparison, all graphs have the same vertical force scale. The symmetric modes have common relative frequency limit between -2.0% and +0.5% of the reference frequency. The antisymmetric modes have their frequency axis limits between -1.0% and +1.0% of the reference frequency.

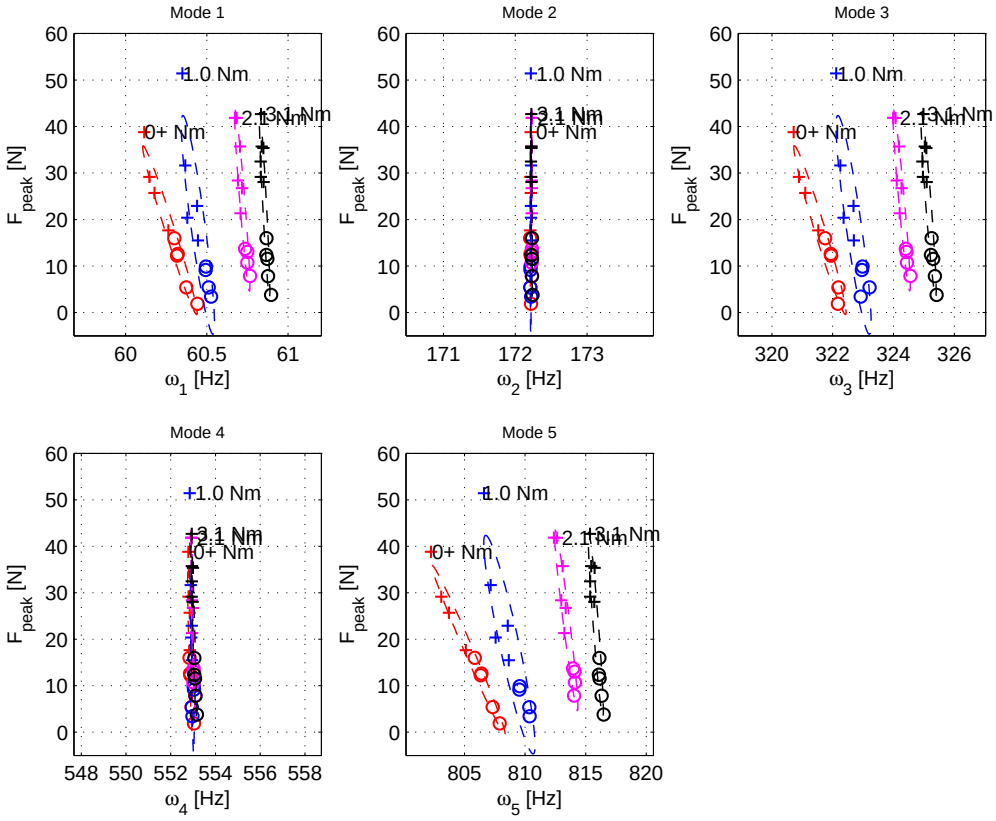

Figure 9: Summary of all frequency identification results.

This figure indicated increased sensitivity of modes S1, S2 and S3 due to joint location relative to the mode shape with mode S3 being the most sensitive to the varying conditions. Increasing torque is responsible for increased natural frequency as well as decreased sensitivity to the changes in the applied force as evidenced by increasingly vertical ellipsoidal frequency clusters. Similar trends are observed in case of all symmetric modes. The antisymmetric modes A1 and A2 are extremely insensitive to the torque variations. The trends in frequency changes for given torque is approximately linear. The case of torque 3.1 Nm represents an asymptotic approach the virtual vertical boundary which would represent the conditions of infinitely stiff or "joint-less" beam of the same shape as the one represented by the assembly contours shown in Figure 1. This condition would represent a linear structure with its frequencies insensitive to the applied excitation.

Further analysis of the joint is performed by means of the relationship between the maximum impact force and the modal damping. These graphs are shown in Figure 10. The style of this presentation is the same as in Figure 9. To facilitate comparison between different modes, the common horizontal damping axis limits are between 0 and 2.8×10^{-3}.

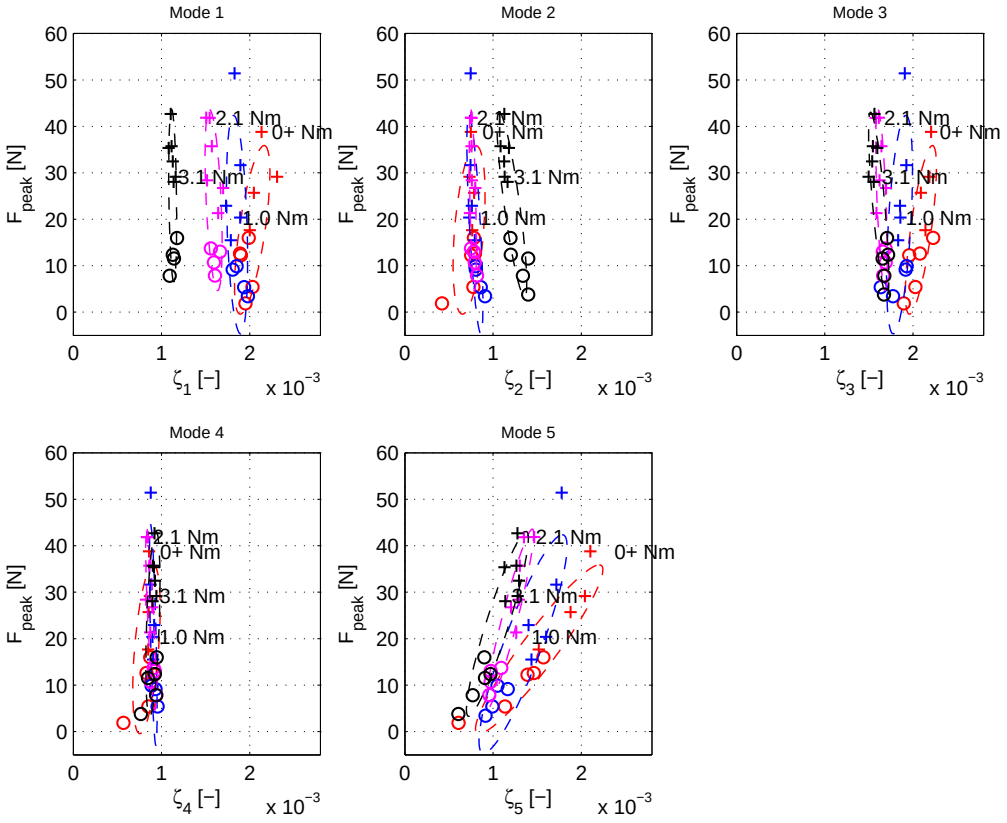

Figure 10: Summary of all damping identification results.

As before, symmetric modes S1, S2 and S3 are generally more sensitive to the applied changes. As expected, the prevalent trend is such that the increased torque causes the reduced damping and reduced force-induced damping variance. This behavior is manifested by more vertical error ellipsoids shifted to the left. This behavior represents decreased damping more linear damping. The damping asymptotically decreases to the background damping caused by the other, more-linear, energy dissipation mechanism such as material damping. Antisymmetric modes A1 and A2 with their mainly vertically oriented error ellipsoids are less sensitive to the joint variations and feature lower damping values. An interesting exception from otherwise consistent trends is the case of mode A1 and torque 3.1 Nm where this torque caused increased damping ratio values. This is either experimental anomaly or an unusual energy dissipation mechanism which would require additional more focused investigations.

Both previous sets of results are combined in one graph to provide damping ratio versus natural frequency *dynamic joint performance maps* with applied forces and torques being the problem parameters. These graphs are shown in Figure 11. The same scaling is used as described in two previous cases. The torque cases are distinguished by using different colors while the force limiting cases are recognizable through the markers used (circle markers represent low peak impact forces and cross markers represent high peak impact forces).

The principal observed trend is that of increasing natural frequency, decreasing damping and decreasing force-induced frequency-damping variance in the tests with increasing tightening torque. Increasing torque influences the position of the measured data clusters, their size and transformation. Anti-symmetric modes A1 and A2 are seen to be frequency-insensitive while the corresponding damping ratios can be considered as being weakly-sensitive to the provided joint changes.

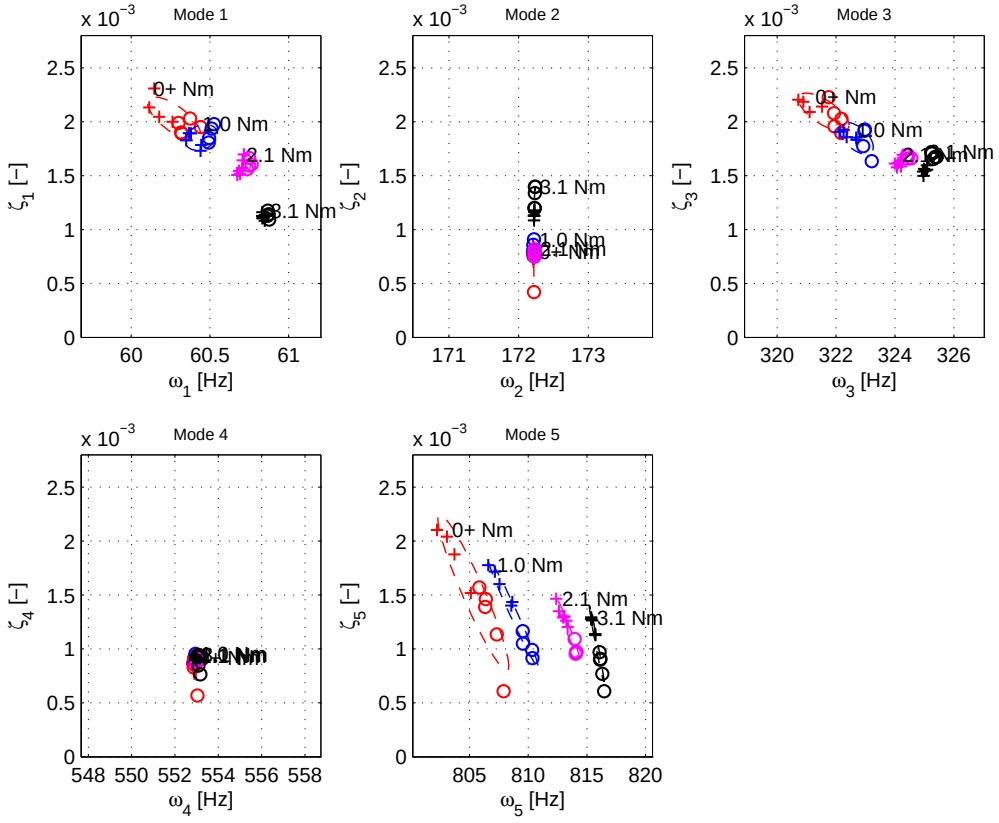

Figure 11: Summary of all identified modal results.

3.3 Analysis of mode 5

Mode 5 is chosen for the more detailed analysis. The *frequency-damping (or modal) performance map* is used to study the properties of this mode when exposed to the changing external conditions. This map is shown in Figure 12a). This is the most sensitive mode with well-defined natural frequency and damping ratio trends. This figure also gives a good indication of the limiting dynamic conditions for the joint. The lowest damping values across all tightening torques correspond to the weakest hammer impacts. These results feature the lowest amount of the anticipated nonlinear effects and the highest presence of experimental noise. The other limiting case is represented by the 0 Nm points. There, the structural link between the two substructures is at its weakest and it causes significant nonlinear effects. These results represent an experimentally observable *boundary case* for the mode. Assuming infinite tightening torque, the joint-induced variance due to changing conditions can be completely suppressed, leading to the condition-independent frequency-damping point in the joint's modal performance map.

Previous observations are outlined in Figure 12b) for mode *i*. The two thick lines represent the zero tightening torque and "zero" impact force boundaries. Point $[\omega_{nj,i},\zeta_{nj,i}]$ represents the "no-joint" and fully linear conditions due to the infinite tightening torque. A joint performance map makes use of these features and it also includes the two families of parametric lines for the conditions with the constant torque and constant impact force. The possibility of *approximate analytical representation* of this generalized performance map is studied next.

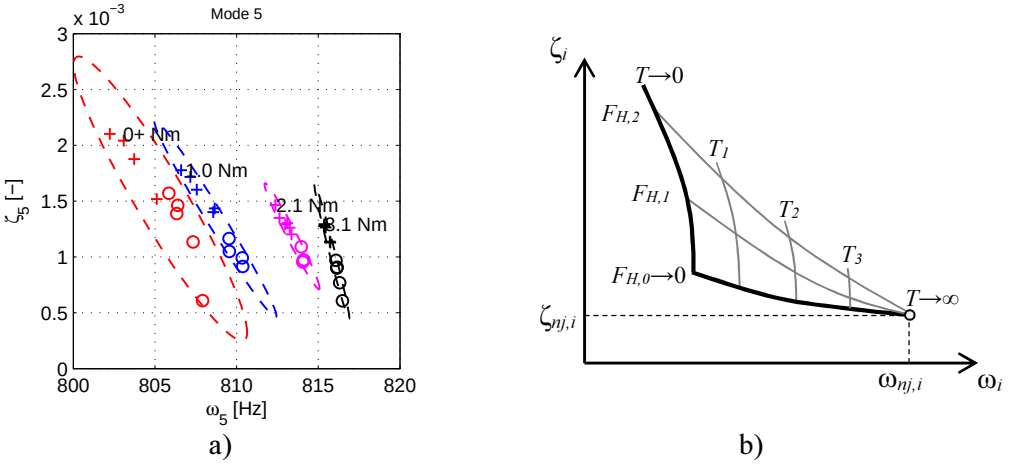

Figure 12: Detail of the frequency-damping map of mode 5 a) and its generalization b).

The joint performance map shown in Figure 12a) is modelled using *quadratic response surfaces* to approximate the identified data $\omega_i(F_H,T)$ and $\zeta_i(F_H,T)$, where F_H is the peak hammer impact force and T is the tightening torque. The full quadratic response model is used

$$\begin{aligned}\omega_j &= f_j(F_H,T) = a_0 + a_1F_H + a_2T + a_3F_HT + a_4F_H^2 + a_5T^2 \\ \zeta_j &= g_j(F_H,T) = b_0 + b_1F_H + b_2T + b_3F_HT + b_4F_H^2 + b_5T^2\end{aligned} \tag{2}$$

where, a_p and b_p are the response function coefficients calculated using all considered test conditions $[F_{H,k},T_l]$ and the linear least square process. The analytical approximation of the measured data has the form $[f_j(F_H,T;a_p),g_j(F_H,T;b_r)]$. The application of this process to mode 5 leads to the response representation shown in Figure 13 for the two dimensional parametric domain $D=F_H\times T$,where $F_H\in[0,35]$ N and $T\in[0,3.1]$ Nm.

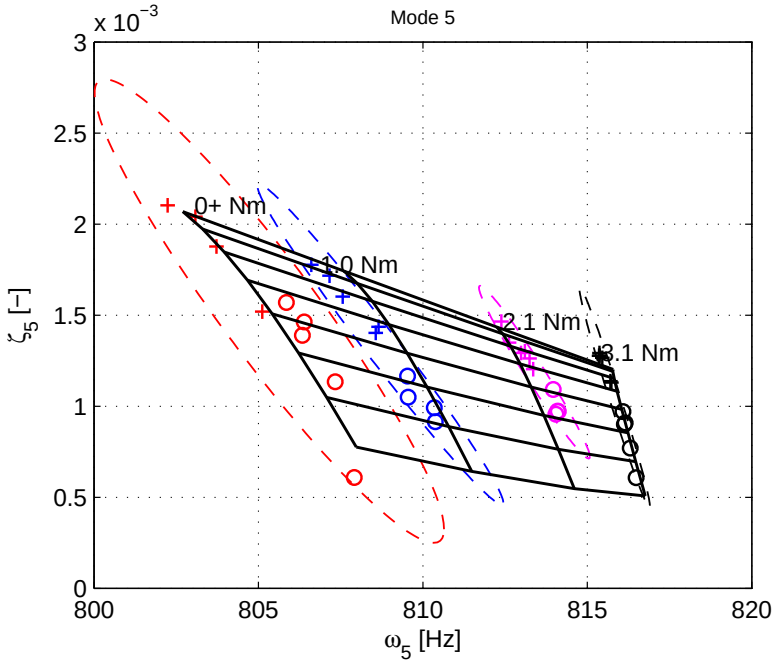

Figure 13: Frequency-damping map of mode 5 and its parameterized response surface representation.

The response surface model is shown as a grid and it is superimposed on the identified frequency-damping data. It captures the main observed trends in the joint's modal performance. Moreover, this model demonstrates a good quantitative correspondence with the experimental data. The identified response surface coefficient, their 95% confidence bounds and the coefficient of determination R^2 [5,9] are presented in Table 1.

	0	1	2	3	4	5	R^2
a_p	807.98	-1.86×10^{-1}	3.83	3.96×10^{-2}	9.96×10^{-4}	-3.22×10^{-1}	0.986257
$a_{p,L}$	807.30	-2.43×10^{-1}	3.25	2.72×10^{-2}	-9.46×10^{-5}	-4.92×10^{-1}	-
$a_{p,H}$	808.70	-1.28×10^{-1}	4.42	5.21×10^{-2}	2.09×10^{-3}	-1.53×10^{-1}	-
b_p	7.75×10^{-4}	5.77×10^{-5}	-1.55×10^{-4}	-5.52×10^{-6}	-5.92×10^{-7}	2.20×10^{-5}	0.933430
$b_{p,L}$	6.48×10^{-4}	4.74×10^{-5}	-2.60×10^{-4}	-7.75×10^{-6}	-7.88×10^{-7}	-8.29×10^{-6}	-
$b_{p,H}$	9.02×10^{-4}	6.80×10^{-5}	-4.94×10^{-5}	-3.29×10^{-6}	-3.98×10^{-7}	5.24×10^{-5}	-

Table 1: Response surface coefficients with their 95% confidence bounds

4 Conclusions

The observed modeshapes feature a class of three symmetric and two asymmetric bending modes. Symmetric modes with high modal amplitudes in the joint region are found to be sensitive to the test parameters. An increase in the tightening torque causes an increase in the identified free response frequencies, while higher the peak impact forces cause a decrease in the values of the natural frequencies. The maximum frequency variation of 2.5% observed in this study corresponds to the third symmetric bending mode. With their values at around 0.2%, the variation of the modal damping is the most pronounced for the third symmetric mode, for which a tightening torque increase causes a decrease in damping, and an increase in the excitation amplitude leads to higher modal damping values.

The methodology presented in this work is aimed at the development of the supporting infrastructure for the design of the reduced order high performance linear joint models. The results presented in this paper will be used in a two-step process based, first, on qualitative and then on quantitative matching between FE joint models and the approximating response surface models of the linearized joint's modal (or dynamic) performance. Such model can be focused either on a particular mode of interest or a specific frequency range which is determined by the number of modes used in the matching process. The regularized sensitivity methods [10] can constitute the basis of the qualitative model design, while the concepts of modal residual correlation [11] can be used as a basis for the quantitative matching.

Acknowledgement

The authors would like to acknowledge Rolls-Royce plc for their support of this research through the Composites University Technology Centre (UTC) at the University of Bristol, UK.

References

[1] E.P. Petrov, D.J. Ewins, *Effects of Damping and Varying Contact Area at Blade-Disk Joints in Forced Response Analysis of Bladed Disk Assemblies*, Journal of Turbomachinery, Vol. 128, ASME DC (2006), pp. 403-410.

[2] E.P. Petrov, D.J. Ewins, *Analysis of essentially non-linear vibration of large-scale models for bladed discs with variable contact and friction at root joints, Proceedings of the 8th International Conference on Vibrations in Rotating Machinery*, Swansea, UK, Swansea (2004), pp. 163-172.

[3] B.M.A. Gowda, H.R. Yeshovanth, C. Siddaraju, *Investigation and Efficient Modeling of an Dovetail Attachment in Aero-engine*, Procedia Materials Science, Vol. 5, Elsevier (2014), pp. 1873-1879.

[4] L. Salles, L. Blanc, F. Thouverez, A.M. Gouskov, *Dynamic analysis of fretting-wear in friction contact interfaces*, Journal of Engineering for Gas Turbines and Power, Vol. 132, ASME DC (2010), pp. 012503-1 - 012503-9.

[5] MATLAB, Software Package, Ver. 8.1, MathWorks, Natick, MA, USA, Natick (2013).

[6] I. Kasa, *A circle fitting procedure and its error analysis*, IEEE Transactions on Instrumentation and Measurement, Vol. IM-25, Issue 1, IEEE (1976), pp. 8-14.

[7] N. Chernov, *Circle Fit (Kasa method),* Available at: http://uk.mathworks.com/matlabcentral /fileexchange/22642-circle-fit--kasa-method-, 2009. [Accessed 10 April 2016]

[8] E. Balmès, *Frequency domain identification of structural dynamics using the pole/residue parametrization, Proceedings of the 14th International Modal Analysis Conference (IMAC)*, Dearborn, USA, Dearborn (1996), pp. 540-546.

[9] R.H. Myers, D.C. Montgomery, C.M. Anderson-Cook, *Response Surface Methodology: Process and Product Optimization Using Designed Experiments*, 4th edition, Wiley-Blackwell (2016).

[10] B. Titurus, M.I. Friswell, *Regularisation in Model Updating*, International Journal for Numerical Methods in Engineering, Vol. 75, Issue 4, John Wiley & Sons Ltd (2008), pp. 440-478.

[11] B. Titurus, M.I. Friswell; *Damage detection using successive parameter subset selections and multiple modal residuals*, Mechanical Systems and Signal Processing, Vol. 45, Issue 1, Elsevier (2014), pp. 193-206.